AGU100 ADVANCING EARTH AND SPACE SCIENCE

Geophysical Research Letters

RESEARCH LETTER
10.1029/2018GL078575

Special Section:
Cassini's Final Year: Science Highlights and Discoveries

Material Flux From the Rings of Saturn Into Its Atmosphere

M. E. Perry[1], J. H. Waite Jr.[2], D. G. Mitchell[1], K. E. Miller[2], T. E. Cravens[3], R. S. Perryman[2], L. Moore[4], R. V. Yelle[5], H.-W. Hsu[6], M. M. Hedman[7], J. N. Cuzzi[8], D. F. Strobel[9], O. Q. Hamil[3], C. R. Glein[2], L. J. Paxton[1], B. D. Teolis[2], and R. L. McNutt Jr.[1]

[1]The Johns Hopkins Applied Physics Laboratory, Laurel, MD, USA, [2]Southwest Research Institute, San Antonio, TX, USA, [3]Department of Physics and Astronomy, University of Kansas, Lawrence, KS, USA, [4]Center for Space Physics, Boston University, Boston, MA, USA, [5]Department of Planetary Sciences, University of Arizona, Tucson, AZ, USA, [6]LASP, University of Colorado Boulder, Boulder, CO, USA, [7]Department of Physics, University of Idaho, Moscow, ID, USA, [8]Ames Research Center, NASA, Mountain View, CA, USA, [9]Department of Earth and Planetary Sciences, The Johns Hopkins University, Baltimore, MD, USA

Abstract During Cassini's final, spectacular months, in situ instruments made the first direct measurements of nanoparticles, finding an exceptionally large flow from the rings into Saturn's atmosphere. Cassini's Ion and Neutral Mass Spectrometer measured material in three altitude bands and found a global-integrated flux of 2–20 $\times 10^4$ kg/s that is dominated by hydrocarbon material $<10^4$u. Ranging from clusters of a few molecules to radii of several nanometers, nanoparticles are ubiquitous throughout Saturn's rings but embedded in the regolith of larger particles and not detectable as independent particles using remote observations. The smallest nanoparticles are susceptible to atmosphere drag by Saturn's tenuous exosphere that reaches the inner edge of the D ring. The unsustainable large flux suggests a recent disturbance of Saturn's inner ring material, possibly associated with the clumping that appeared in the D68 ringlet in 2015.

Plain Language Summary For 40 years, calculations based on remote observations indicated that Saturn's magnetic field carries ions and charged particles from the rings to the midlatitudes of Saturn. In Cassini's last few months of life, direct, in situ measurements found that 10 tons/s of molecules and particles smaller than two nanometers are streaming along the plane of the rings into Saturn's atmosphere by another process: atmospheric drag. Saturn's extended atmosphere reaches the inner edge of Saturn's rings and extracts neutral particles less than one thousandth the thickness of a human hair by slowing them down until they fall into Saturn. Surprisingly, the flux is a hundred times larger than past predictions, and at least half of the material is hydrocarbon, which comprises less than 5% of the water ice-dominated rings. Cassini's data also show that the influx varies at least a factor of 4 and may be linked to clumps that appeared in 2015 on D68, the ringlet on the inner edge of the rings. These newly discovered particles and processes alter the evolutionary landscape of the rings and provide an exciting, rich field for future research aimed at understanding the origin and history of the rings.

Key Points:
- Atmospheric drag, an interaction newly applied to Saturn and its rings, extracts $>10^4$ kg/s of neutral nanoparticles from Saturn's rings
- Molecules and particles <2 nm in radius are preferentially transported by atmospheric drag
- Neutral, nanometer-sized hydrocarbon material is currently the largest mass loss from Saturn's rings

Supporting Information:
- Supporting Information S1

Correspondence to:
M. E. Perry,
mark.perry@jhuapl.edu

Citation:
Perry, M. E., Waite, J. H., Jr., Mitchell, D. G., Miller, K. E., Cravens, T. E., Perryman, R. S., et al. (2018). Material flux from the rings of Saturn into its atmosphere. *Geophysical Research Letters*, *45*. https://doi.org/10.1029/2018GL078575

Received 8 MAY 2018
Accepted 31 JUL 2018

1. Introduction

Forty years before Cassini in situ observations directly measured material influx from Saturn's rings, Connerney and Waite (1984) deduced its existence from the depressed electron densities in Saturn's ionosphere, measured during Pioneer and Voyager radio frequency occultations. Analyses of subsequent ground-based observations (Moore et al., 2015) further quantified the global-integrated flux at 5–20 kg/s and determined that the highest flux was at lower latitudes, within 30° of the equator. Extensive research (Hsu et al., 2016; Ip et al., 2016; Jontof-Hutter & Hamilton, 2012; Northrop & Connerney, 1987) modeled the posited transport mechanisms for charged ice grains and water ions that are sputtered from the rings and flow along Saturn's magnetic field lines. These models showed that most of the influx is via charged ions and nanoparticles at Saturn's midlatitudes, between 40 and 70°, the latitudes that connect magnetic field lines to the rings.

As reported in Hsu et al. (2018), Mitchell et al. (2018), and Waite et al. (2018), Cassini's in situ observations showed an influx with a charge, composition, transport process, and quantity that is dramatically different from predictions. Neutral hydrocarbon material, extracted from the rings, enters primarily in a tight stream along the equatorial plane. In this paper, we describe the Ion and Neutral Mass Spectrometer (INMS) data

and then provide a description of the influx as constrained by those data. We discuss the total mass flux, partitioning of the flux between molecules and particles, dispersion and diffusion of the flux as derived from high-altitude and low-altitude data, implications for the size-frequency distribution of the incoming particles, and characteristics of the atmospheric-drag transport processes that deliver the molecules and particles from the rings to Saturn's upper atmosphere.

A few notes on usage: altitudes are the heights above the 1-bar level as defined by an oblate spheroid (Archinal et al., 2011). The material measured by INMS contains primarily hydrogen and carbon atoms, and we refer to the material as hydrocarbons although other organic material may be present. The accompanying supporting information document contains additional nomenclature, uncertainties, and analysis details.

2. Proximal Data

2.1. INMS Instrument

All the measurements of neutrals were gathered using the INMS Closed Source Neutral (CSN) mode (Waite et al., 2004). Incoming material enters the CSN antechamber and then travels along a transfer tube to the ionization chamber where it is ionized, mass filtered through a quadrupole analyzer, and then counted. The CSN mode has a 2π field of view which simultaneously captured both orbiting and atmosphere material. There are two characteristics of the CSN mode that are important for interpreting INMS measurements during proximal orbits. (1) To reach the ionization chamber, a molecule requires ~100 contacts with the walls of the inlet system (Teolis et al., 2010), so only volatiles can be measured. Reactive neutrals such as OH and silicate molecules will adhere to the walls and not be measured. Volatiles with some affinity for adhesion take longer to pass through the inlet system, and their count rates are suppressed and extended. (2) At 30 km/s, the impact velocity of the incoming material is 5 times the velocity of the Titan passes for which INMS was designed. Each nucleon carries 5.1 eV of energy that is partitioned between heating the CSN wall, dissociating the incoming molecule or particle, and suppling internal and kinetic energy to the rebounding molecule or fragments. Particles and large molecules will fragment, so the spectra measured by INMS (Waite et al., 2018) represent the volatile fragments of the incoming molecule or particle. The maximum mass directly measured by INMS is 100 u, and the original composition and mass of larger molecules or particles must be deduced from fragments that are within the INMS mass range and other data.

2.2. Cassini Proximal Orbits

We group INMS data by orbit into high, middle, and low bands that are based on the orbit periapsis altitudes, which range from 1,370 to 3,600 km. Each orbit is nearly polar, north to south, with the lowest altitude reached at $-6°$latitude near local noon. The last encounter, the final plunge, which is part of the low-altitude group, occurred at higher latitudes (9–15°) and progressed to slightly lower altitudes, 1,370 km, before Cassini lost contact with the Earth. Table S1 shows the equatorial crossing and minimum altitudes for each group.

2.3. INMS Data

Except for hydrogen from Saturn's atmosphere, the contents of the neutral spectra from the high-altitude (3,400- to 3500-km periapsis) orbits were entirely unexpected (Figure 1a). The predicted water flux was below the INMS detection limit, so its absence was disappointing but not unforeseen. But the surprising presence of methane and a 28-u species was only explained later when we understood that the rings provide a source of material. The INMS inlet system suppresses water due to its adsorption to the wall followed by a slow release. By analyzing postencounter data, we find that water at this altitude has approximately the same abundance as the methane within a factor of 2. CH_4 is unambiguously identified by its ionization dissociative pattern, and C_2H_4 is 25–30% of the 28-u measurement, with N_2 and CO as possible molecules for the remaining material. (Later, we discuss whether these measurements are native molecules or fragments.) For masses heavier than 44 u, no single mass had measurements more than 1 sigma above the noise level. Adding all of the higher masses together does reveal signal above the background, with 10–20% of the total abundance of material in the higher masses. CH_4 and the species with a mass of 28 u have very different distributions (Figure 1b), with neither peaking at the lowest altitude. The clear bias of the 28-u species toward the equator is the first indication that the material is entering Saturn at the equator.

Data at middle altitudes (2,700–3,000 km) are similar in composition to the higher-altitude data but are ifferent in two important respects: the latitudinal distribution has lost most of its bias toward the equator,

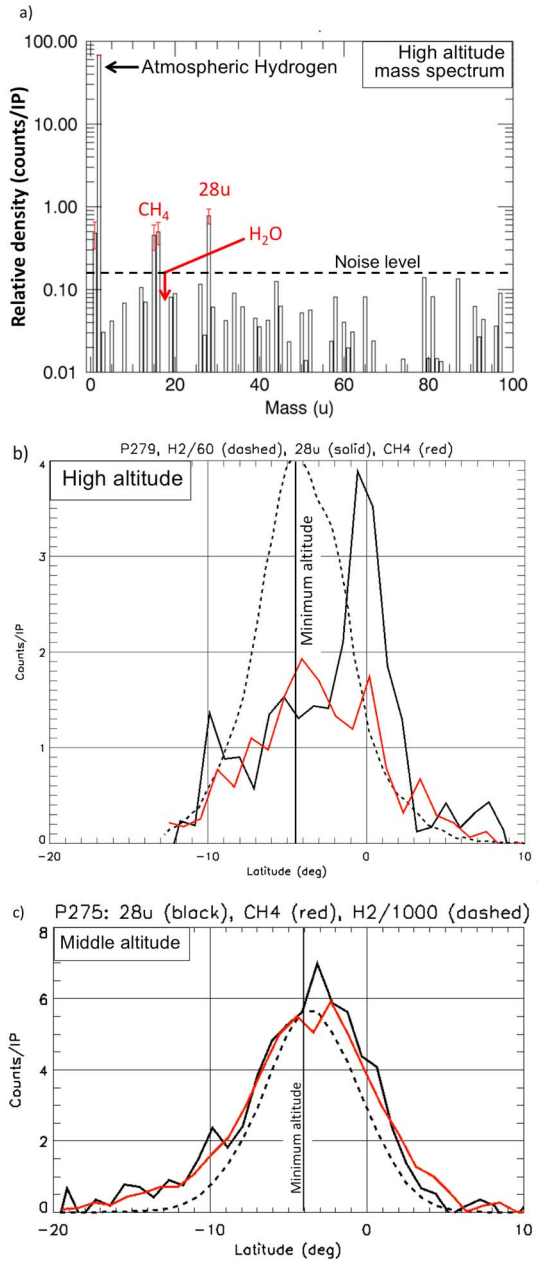

Figure 1. (a) Mass spectrum from a high-altitude pass, orbit 278. Uncertainties are shown as red error bars on each mass; masses without error bars are less than 1σ above the noise. (b) Latitude distribution of the three primary species, H_2 (scaled to match the 28-u peak), CH_4, and 28u. Each measurement has an uncertainty of 15% to 25%. (c) The 28-u and H_2 (atmosphere) distributions for a middle-altitude pass, orbit 274, showing only a slight bias toward the source of the influx at the equator.

and the mixing ratio of the minor species is lower (Figure 1c). Although the atmospheric density has increased a factor of 30, the densities of the minor species are only twice that of the higher altitudes. The altitude of these measurements is the closest match to the altitude of the Ion and Neutral Camera (INCA) detection of particles (see section 2.5).

Combining the high- and middle-altitude data provides information sufficient to determine that the source of the minor species is from above the atmosphere and that the material enters along the ring plane. The equatorial mixing ratios (Figure S1) for 28 u decrease from >0.5% at the highest measured equatorial altitude, 3,500 km, down to <0.02% at 2,800 km, the altitude of the exobase, where collisions with the atmosphere's H_2 molecules determine behavior of minor species. Moreover, at high altitudes, the equatorial mixing ratios for the 28-u species are 6 times the ratios 5° from the equator (Figure 1b), placing the material source at the ring plane.

At low altitudes, INMS shows a complex hydrocarbon spectrum (Waite et al., 2018, and Figure S2), that likely consists of the volatile fragments of larger particles. Water is also present. Waite et al. (2018) report on the composition. The predominance of hydrocarbons over water, the primary ring material, may be linked to the particle size distribution, which is discussed in section 3.3. The peak densities of the minor species are ~1,000 times higher than those measured during the high-altitude passes. At these altitudes, each species tracks the density of the hydrogen atmosphere with the exception of HD and helium, which both diffuse up from Saturn's lower atmosphere. The densities and mass flux are discussed in the analysis section.

2.4. Variability

During the proximal orbits, the low-altitude mixing ratios varied independently of the H_2 density. This is particularly evident in CH_4, where the mixing ratio varied a factor of 3 from pass to pass (Waite et al., 2018), and in the total integrated mass, which varied by a factor of 4 from the lowest total (orbit 288) to the highest total (orbit 291). Some of the passes also showed an asymmetry in the CH_4 distribution that can be attributed to a change in flux within a few diffusion time scales (Figure 2). This variability provides clues to source of the influx. As described by Waite et al. (2018), at least a portion of this variability appears to be linked to the clumps of material in the D68 ringlet. The CH_4 variations were not associated with Saturn longitude or local time.

2.5. Additional Data From the MIMI

We describe Magnetospheric Imaging Instrument's (MIMI) data (Krimigis et al., 2004) because they are crucial to interpreting INMS observations. Mitchell et al., 2018 analyzes INCA measurements of particles with masses $>1 \times 10^4$ u, a local density of 0.1/cm^3, and a smooth distribution centered on the equator with a half width of 1.4°. Each of the three orbits where INCA collected data was in the middle-altitude band from 2,850 to 3,150 km, and the measurements from each set of data were identical, showing that the population is well defined and stable, in contrast to the variability observed in CH_4 and in the total mass flux that is described in the next section. For spherical particles with density of 1 g/cm^3, the mass range corresponds to radii of 1.6–2.5 nm. At low altitude, another MIMI instrument, the CHarge Energy Mass Spectrometer, finds similarly sized particles that are positively charged, demonstrating that many of the higher-altitude particles observed by INCA survive to low altitudes, as predicted by simulations such as those by Hamil et al. (2018).

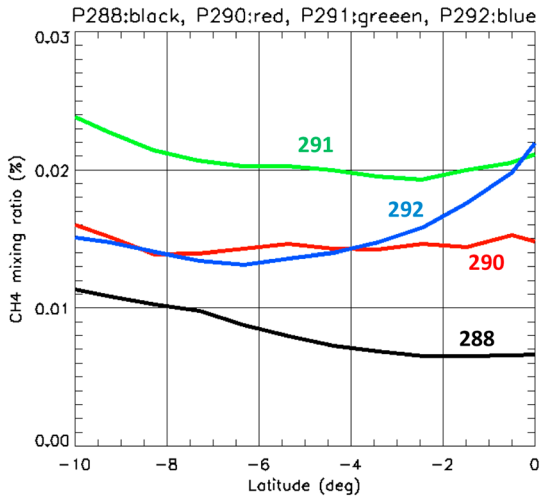

Figure 2. The CH_4 abundance shows temporal variability on scales of hours. As the CH_4 diffuses into Saturn's atmosphere, the CH_4 mixing ratios reflect both the current and past influx rates. The equatorial ratio shows the most recent influx rate, and the ratios farther from the equatorial source show past rates, or hours earlier for the latitudes of this plot. At the time of orbits 288 and 291, influx had recently been higher. Orbit 290 shows a constant flux, and orbit 292 reflects an influx that is increasing.

3. Analyses

3.1. Saturn's Rings as the Source of Material

The altitude and latitude dependence of minor species are assessed by comparing their densities to the H_2 density, which has a known altitude dependence. When the species density profile deviates from H_2 as in Figure 1b, that indicates variations with latitude. Similarly, a constant mixing ratio indicates no latitude dependence. Variable flux may also cause deviations from H_2, so multiple orbits are used to confirm the latitude dependence.

Altitude and latitude dependence of the mixing ratios identify the rings as the source of the minor species measured by INMS. This conclusion is further bolstered by the INCA-measured particles and the atmospheric-drag simulation reported in Mitchell et al. (2018) that reproduces the INCA results. In the simulation, molecules at the D68 ringlet (Hedman et al., 2014) on the inner edge of the D ring are extracted by collisions with Saturn's extended H atmosphere (see Broadfoot et al., 1986 for similar analysis at Uranus). The collisions de-orbit the particles by reducing their periapses to below Saturn's exobase, and material enters Saturn's upper atmosphere within 2 hr (half of a Kepler orbit period) from the first few collisions. This process extracts molecules and nanoparticles with radii less than ~5 nm. For larger particles, charging times by photoionization or by local plasma collisions become comparable or shorter than the time for a sufficient number of collisions to de-orbit the particle. This time scale is important as atmospheric-drag transport is contingent on the particles remaining uncharged until entering Saturn's atmosphere. Charged molecules and particles may still enter Saturn's atmosphere, but the mechanism and entry location are affected by the magnetic field (see Hsu et al., 2017; Ip et al., 2016; Northrop & Connerney, 1987, for analyses of the dynamics of larger nanoparticles and micrometer-sized particles).

The dispersion or spread of material at altitudes above the exobase depends on the mass of the material, and the spatial distributions of the INMS data have signatures of both particle and molecule influx from the rings. Simulations of atmospheric drag predict that the dispersion of 2- to 3-nm particles is $<2°$, in agreement with the ±1.4° latitude range measured by INCA. Predictions for the larger spread of lighter CH_4 are 4–5°, a result that we use to identify the INMS-measured CH_4 as molecular because the distribution at high altitudes matches this 4–5° (Figure 1b). The main component of the INMS-measured 28-u distribution is narrow, centered at the equator, and is indistinguishable from the distribution of INCA particles, leading to the conclusion that particles or relatively massive molecules supply a substantial portion of the material for the 28-u fragments. There is, though, additional 28-u signal that is broader, similar to the CH_4 distribution, and that appears to be additional native species such as N_2 or CO molecules that are lighter than the heavy particles and that contribute to the 28-u measurements. Below the exobase, interactions with the atmosphere control the majority of the material, and the distributions of all INMS-measured material have the same scale height as the atmosphere, as expected for infalling material (see next section).

Variability of CH_4's mixing ratio is further confirmation that the rings are the source of material. Orbit-to-orbit variations in CH_4's mixing ratios may be associated with the location of the bright clumps in the D68 ringlet (Waite et al., 2018). Variations within a single low-altitude pass are a signature of the rapid change in flux that a spatially or temporally varying source produces. At the 340 to 370 K temperatures of Saturn's atmosphere (Moore et al., 2018; Yelle et al., 2018), the vertical diffusion of CH_4 is several hours, and the spatial dependence of the mixing ratio reflects the change in the source.

3.2. Mass Flux, Velocities, and Material Sizes

Converting the local densities to mass flux requires estimates of the vertical velocities, which vary with altitude and with the mass and size of the entering particle or molecule. For the lower measured altitudes,

below the exobase (2,800–3,200 km), there are sufficient collisions to control the species velocity and diffusive velocities are appropriate. Considering that the ring material is flowing into Saturn's atmosphere by gravity without any upward opposing pressure, a particle or molecule with radius a, if $a << $ mean free path, is settling in the Epstein (kinetic) regime by viscous drag with a sedimentation, terminal velocity of

$$v_s = \frac{0.36\rho_p g(2a)}{m_{H2} n_{H2} v_{H2}} \quad (1)$$

where v_s is the sedimentation or terminal velocity; ρ_P is the mass density of the particle or molecule and $2a$ is its diameter; v_{H2}, n_{H2}, and m_{H2} are the mean thermal speed, density, and mass of H_2; and g is the gravitational acceleration (Sagan & Chyba, 1990). The density of Saturn's atmosphere increases almost 1,000-fold from the exobase to 1,600-km altitude, and the sedimentation velocity decreases by the same factor. For molecules, the sedimentation velocities equate to the maximum diffusion velocity, which assumes that the diffusing material has the same scale height as the atmosphere (cf. Banks & Kockarts, 1973, and section S4).

With their inverse dependence on atmosphere density, all infalling molecules and particles that reach terminal velocity have the same scale height as the atmosphere. Since material diffusing upward from the homopause have mass-dependent scale heights (see helium in Waite et al., 2018), the match between the scale heights of minor species and H_2 is further an indication that the material enters Saturn's atmosphere from the top.

We calculated velocities assuming that all the materials are molecules, an assumption that provides a lower bound for velocities and fluxes and that is acceptable because the apportioning of material between molecules and heavier particles is only weakly constrained. The velocities of molecules for the 1,700-km, low-altitude band are 10–30 m/s depending on the cross section and mass of the species. At low altitudes, the assumed latitude spread, ±10°, is based on volatile masses such as CH_4, 58u (C_4H_{10}), and C_6H_6, which have mixing ratios that appear unchanged from the equator to −10° of latitude. Using the INMS densities, we find that the total flux of INMS-measured material is 1 to 20×10^4 kg/s (Table S2), consistent with independent analyses reported by Yelle et al. (2018) and Waite et al. (2018). The broad range is due to a fourfold variation in the flux and to uncertainties, primarily in velocities and latitude extent of the minor species at low altitude.

Flux into Saturn should be conserved, so we perform an additional check on the flux by estimating it at the middle altitude band (3,000-km periapses), which is also the altitude of INCA data and is near the exobase. Uncertainties at this altitude are larger due to the lower signal levels and to the difficulty in determining velocities near the exobase, where material falling in from the rings has experienced relatively few collisions and the molecules are either in ballistic trajectories or satellite orbits. The distributions and concentrations are relatively constant in the exosphere. Indeed, CH_4 and 28-u densities are nearly unchanged between altitudes of 4,000 and 3,000 km, indicating that the particles are still above the exobase and free falling. In this region and at the exobase, Monte Carlo calculations of atmospheric drag produce the vertical velocity from the number of high-altitude collisions and the exchange of momentum that causes the material to deorbit.

The fluxes estimated at the middle-altitude band are approximately 50% lower than at low altitudes, and this difference can be ascribed to the likelihood that some material is unobserved by INMS at the middle altitude. Although the densities in Table S2 do include the barely detected masses heavier than 44 u, many of these masses are undetectable due to wall adhesion, an effect that is observed during low-altitude measurements. To investigate the possibility of underrepresenting higher masses, we partition the observed spectra into mass bins (Figure S3) and set the velocity parameters so that the total integrated mass flux of CH_4, the dominant volatile, is equal at both 1,700 and 3,000 km. Comparing the other species shows that many of the molecules with masses >28 u were not captured in the 3,000-km data.

The global-integrated flux of $>10^4$ kg/s is 3 orders of magnitude larger than most predictions (Moore et al., 2015; Northrop & Connerney, 1987) and a convincing argument that the present-day, measured flux is epoch dependent. Even the lower bound, 10^4 kg/s, is unsustainable for less than 10^6 years without depleting the entire ring system of hydrocarbons and all of the mass in the D ring. From studies of ring contamination, the age of the rings is at least tens of millions of years (Cuzzi & Estrada, 1998). The INMS-measured flux must therefore be much larger than the average flux over the lifetime of the rings, and the clumps that appeared in D68 in 2015 are excellent candidates for recent enhancement of material influx (Hedman & Showalter, 2016).

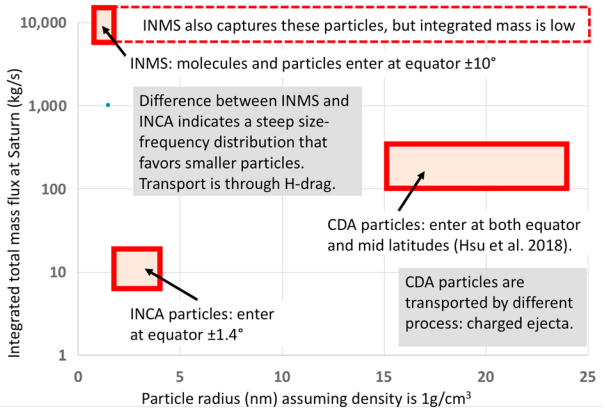

Figure 3. INMS, INCA (Mitchell et al., 2018), and CDA (Hsu et al., 2018) measure particles with different masses. The INCA particles, >10,000u, constitute only a small fraction of the flux observed by INMS. The high flux for INMS indicates a steep size-frequency distribution. INMS measures material at all masses, but most of the mass is in lighter, smaller material. INMS = Ion and Neutral Mass Spectrometer; INCA = Ion and Neutral Camera.

Additional evidence that the influx has been recently released from collisions in the rings is the large flux of highly volatile CH_4 because there are no known mechanisms that produce large amounts of CH_4, and its volatility leads to rapid loss if it is brought to the rings.

The authors acknowledge the massive, unexpected, and unsustainable size of this flux. Multiple diligent, careful reviews of the data, analyses, and instrumental effects were unable to reduce the flux below 10^4 kg/s. In fact, a flux 10 times larger is consistent with the data.

The INCA data and the distribution of 28-u measurements at the highest altitudes indicate that some of the material measured by INMS is likely heavier particles. When more massive than 5,000 u, particles do not slow to atmospheric diffusion velocities until well below the exobase. These particles will not have the scale height of H_2. In contrast, the lighter molecules from the D ring experience sufficient collisions to quench their orbital velocity at 3,500 km or above. Since most of the material measured by INMS is diffusively coupled to the atmosphere below the exobase, the native material must be molecules or particles smaller than approximately 500 u. From the 28-u distribution at high altitude, the upper limit on the amount of total material that is likely due to heavier particles is 20% to 30%, similar to that inferred by Waite et al. (2018). At the same altitudes, the CH_4 appears to be molecular and comprises 10% to 20% of the mass. The distribution of the remaining mass, approximately half of the total mass, is not characterized at the high altitudes. The 200- to 500-u average mass of the material (see supporting information) would satisfy the steep size-frequency distribution (next section) and the rapid diffusion of material below the exobase.

It is interesting to compare these proximal data to the INMS measurements from the ring-grazing orbits at 2.4 R_S from Saturn. The dominant species are the same, H_2, CH_4, 28 u, and 44 u, with 28-u molecules comprising most of the mass. Within measurement error, all the masses measured during these ring crossings have identical spatial distributions, which marks them as nanoparticle fragments rather than as molecules, which would all have spatial distributions that differed from each other. The distributions were stable during the 4 months of measurements, and the mass density of the nanoparticles was 10^5 u/cm^3, similar to the densities at Saturn above the exobase. Apparently, nanoparticles are ubiquitous throughout the gaps in Saturn's rings.

3.3. Size-Frequency Distribution and Source Parameters

When compared to INCA—which cannot measure particles less massive than 10^4 u—and Cassini Cosmic Dust Analyzer results (Figure 3), the INMS-derived, global-integrated flux of $>10^4$ kg/s indicates an exceptionally steep size-frequency distribution for the smaller material. The INCA-measured particles—which are also measured by INMS—provide only a small fraction of the total mass flux. A hypothesis that explains this apparent discrepancy is that most of the INMS-measured mass must be in molecules and small particles. The lack of variation in the INCA measurements shows that they are decoupled from the CH_4 and from the bulk of the mass flux, additional evidence that most of the mass is in smaller particles or individual molecules. We use the power relationship for the size-frequency distribution, $n(r) \propto r^{\alpha}$, to explore the data. Fragmentation distributions for particles with radii larger than a micron are usually described using $\alpha = 3$ or 4, but α may be 6 or larger based on the difference between the INCA and INMS fluxes.

Three processes determine the size-frequency distribution of particles measured in Saturn's atmosphere: the source distributions from the phenomena that create the particles, transport processes, and loss mechanisms. Most small particles in Saturn's rings are created by meteoroid impact. The size distributions of these ejecta are usually described using $\alpha = 3$ or 4, and that may be appropriate for the entire range of sizes, from large particles down to molecular clusters. Small particles may then adhere to each other to create larger ones, but this would increase the proportion of large particles, and the source processes are not a clear cause of the disproportionally large number of small particles. Another possible light-molecule enhancement is a small-particle population with unusually large areas (e.g., fractal aggregates), and these would de-orbit

faster. Currently, there are no data that suggest that the lower-mass particles are unusually large or have low density.

The steep size-frequency distribution can be explained by comparing the two processes that can transport material from the rings to Saturn: the well-studied process that carries charged material into Saturn primarily along magnetic field lines (see references in the introduction) and atmospheric drag that moves neutral material along the ring plane (Mitchell et al., 2018). INMS-measured neutral particles are transported by the gas-drag process, which preferentially transports smaller particles for two reasons: (1) particles larger than tens of nanometers are barely affected by the sparse atmosphere and (2) charging time is proportional to particle area, so smaller particles remain neutral longer. For particles up to tens of nanometers, transportation is determined by how quickly a particle can acquire an electric charge. Once charged, the electromagnetic forces become much more important than gas drag. This qualitatively fits the trend as shown in Figure 3, which shows that most of the neutral flux along the equatorial plane are smaller particles. Analyses are ongoing to provide further details on the transport of these small particles.

The ultimate source of these refractory organic nanoparticles is probably tiny inclusions within much larger, 10- to 100-μm ring regolith particles. The embedded hydrocarbon motes give the ring particles their reddish color (Ciarniello et al 2018; Cuzzi et al., 2018) and may date back to the ring parent. The nanoparticles become liberated from their icy sheath by photosputtering of the water of ejected chips (Hsu et al., 2018). The degree to which the hydrocarbon nanoparticles immediately mix back into another ring particle surface at the same location, or slowly evolve inward (Salmon et al., 2010) to concentrate increasingly at smaller radii (Hedman et al., 2013), is an excellent subject for future study.

4. Conclusion

During Cassini's Grand Finale, INMS acquired data that are sufficient to characterize the altitude and latitudinal distributions in the vicinity of Saturn's equator of a flux of material from Saturn's rings. At $>10^4$ kg/s, the enormity of the mass flux implies its time-dependent nature and, combined with the observed variability, links the influx to the clumps that appeared in the D68 ringlet in 2015. The predominance of hydrocarbons is unexpected and awaits a comprehensive explanation. Neutral nanoparticles with radii <3 nm radius are plentiful in the inner D ring, and the bulk of the influx is currently composed of small neutral particles, not charged particles or ions. The INMS data indicate that the role of nanoparticles in mass redistribution within the rings may be larger than previously assumed.

Acknowledgments
The work was supported by NASA contract to SwRI, NAS703001TONMO711123, JPL subcontract 1405853, and APL grants NNX13AG63G, NNX13AH83G, and NNX16AI50G. D. F. S. was supported by the Cassini-Huygens Mission through JPL contract 1408487. All data used in this research are available from the Planetary Data System archive.

References

Archinal, B. A., A'Hearn, M. F., Bowell, E., Conrad, A., Consolmagno, G. J., Courtin, R., et al. (2011). Report of the IAU working group on cartographic coordinates and rotational elements: 2009. *Celestial Mechanics and Dynamical Astronomy*, *109*(2), 101–135. https://doi.org/10.1007/s10569-010-9320-4

Banks, P. M., & Kockarts, G. (1973). *Aeronomy*. New York: Academic Press.

Broadfoot, A. L., Herbert, F., Holberg, J. B., Hunten, D. M., Kumar, S., Sandel, B. R., et al. (1986). Ultraviolet spectrometer observations of Uranus. *Science*, New Series, *233*(4759), 74–79.

Ciarniello, M., Filacchione, G., D'Aversa, E., Capaccioni, F., Nicholson, P. D., Cuzzi, J. N., et al. (2018). Cassini-VIMS observations of Saturn's main rings: II. A spectrophotometric study by means of Monte Carlo ray-tracing and Hapke's theory. *Icarus*, *317*, 242–265. https://doi.org/10.1016/j.icarus.2018.07.010

Connerney, J., & Waite, J. (1984). New model of Saturn's ionosphere with an influx of water from the rings. *Nature*, *312*(5990), 136–138. https://doi.org/10.1038/312136a0

Cuzzi, J. N., & Estrada, P. R. (1998). Compositional evolution of Saturn's rings due to meteoroid bombardment. *Icarus*, *132*(1), 1–35. https://doi.org/10.1006/icar.1997.5863

Cuzzi, J. N., French, R. G., Hendrix, A. R., Olson, D. M., Roush, T., & Vahidini, S. (2018). HST-STIS spectra and the redness of Saturn's rings. *Icarus*, *309*, 363–388. https://doi.org/10.1016/j.icarus.2018.02.025

Hamil, O., Cravens, T. E., Reedy, N. L., & Sakai, S. (2018). Fate of ice grains in Saturn's ionosphere. *Journal of Geophysical Research: Space Physics*, *123*, 1429–1440. https://doi.org/10.1002/2017JA024616

Hedman, M. M., Burt, J. A., Burns, J. A., & Showalter, M. R. (2014). Non-circular features in Saturn's D ring: D68. *Icarus*, *233*, 147–162. https://doi.org/10.1016/j.icarus.2014.01.022

Hedman, M. M., Nicholson, P. D., Cuzzi, J. N., Clark, R. N., Filacchione, G., Capaccioni, F., & Ciarniello, M. (2013). Connections between spectra and structure in Saturn's main rings based on Cassini VIMS data. *Icarus*, *223*(1), 105–130. https://doi.org/10.1016/j.icarus.2012.10.014

Hedman, M. M., & Showalter, M. R. (2016). A new pattern in Saturn's D ring created in late 2011. *Icarus*, *279*, 155–165. https://doi.org/10.1016/j.icarus.2015.09.017

Hsu, H.-W., Kempf, S., Badman, S. V., Kurth, W. S., Postberg, F., & Srama, R. (2016). Interplanetary magnetic field structure at Saturn inferred from nanodust measurements during the 2013 aurora campaign. *Icarus*, *263*, 10–16. https://doi.org/10.1016/j.icarus.2015.02.022

Hsu, H.-W., Horányi, M., & Kempf, S. (2017). On the time-dependent grain charging and its effects on ring-atmosphere interactions at Saturn. In C. M. Ko, P. C. Yu, & C. K. Chang (Eds.), *Serendipities in the solar system and beyond – Celebrating Prof. Wing-Huen Ip's 70th birthday*. ASP Conference Series, 513, 177–181. San Francisco, CA: Astronomical Society of the Pacific. ISBN: 978-1-58381-910-4

Hsu, H.-W., Schmidt, J., Kempf, S., Postberg, F., Moragas-Klostermeyer, G., Seis, M., et al. (2018). Cosmic dust analyzer onboard Cassini collects material from Saturn's main rings. *Science*. https://doi.org/10.1126/science.aat3185

Ip, W.-H., Liu, C.-M., & Pan, K.-C. (2016). Transport and electrodynamical coupling of nano-grains ejected from the Saturnian rings and their possible ionospheric signatures. *Icarus*, *276*, 163–169. https://doi.org/10.1016/j.icarus.2016.04.004

Jontof-Hutter, D., & Hamilton, D. P. (2012). The fate of sub-micron circumplanetary dust grains I: Aligned dipolar magnetic fields. *Icarus*, *218*(1), 420–432. https://doi.org/10.1016/j.icarus.2011.09.033

Krimigis, S. M., Mitchell, D. G., Hamilton, D. C., Livi, S., Dandouras, J., Jaskulek, S., et al. (2004). Magnetosphere imaging instrument (MIMI) on the Cassini mission to Saturn/Titan. *Space Science Reviews*, *114*(1–4), 233–329. https://doi.org/10.1007/s11214-004-1410-8

Mitchell, D. G., Perry, M. E., Hamilton, D. C., Westlake, J., Kollmann, P., Smith, H. T., et al. (2018). Dust grains fall from Saturn's D-ring into its equatorial upper atmosphere. *Science*. https://doi.org/10.1126/science.aat2236

Moore, L., O'Donoghue, J., Müller-Wodarg, I., Galand, M., & Mendillo, M. (2015). Saturn ring rain: Model estimates of water influx into Saturn's atmosphere. *Icarus*, *245*, 355–366. https://doi.org/10.1016/j.icarus.2014.08.041

Moore, L., Cravens, T. E., Müller-Wodarg, I., Perry, M. E., Waite, J. H., Perryman, R. S., et al. (2018). Models of Saturn's equatorial ionosphere based on in situ data from Cassini's grand finale. *Geophysical Research Letters*, *45*. https://doi.org/10.1029/2018GL078162

Northrop, T. G., & Connerney, J. E. P. (1987). A micrometeorite erosion model and the age of Saturn's rings. *Icarus*, *70*(1), 124–137. https://doi.org/10.1016/0019-1035(87)90079-0

Salmon, J., Charnoz, S., Crida, A., & Brahic, A. (2010). Long-term and large-scale viscous evolution of dense planetary rings. *Icarus*, *209*(2), 771–785. https://doi.org/10.1016/j.icarus.2010.05.030

Sagan, C., & Chyba, C. (1990). Triton's streaks as windblown dust. *Nature*, *346*(6284), 546–548.

Teolis, B. D., Perry, M. E., Magee, B. A., Westlake, J., & Waite, J. H. (2010). Detection and measurement of ice grains and gas distribution in the Enceladus plume by Cassini's Ion Neutral Mass Spectrometer: Enceladus plume structure from INMS. *Journal of Geophysical Research*, *115*, A09222. https://doi.org/10.1029/2009JA015192

Waite, J. H., Lewis, S., Kasprzak, W. T., Anicich, V. G., Block, B. P., Cravens, T. E., et al. (2004). The Cassini ion and neutral mass spectrometer (INMS) investigation. *Space Science Reviews*, *114*(1–4), 113–231. https://doi.org/10.1007/s11214-004-1408-2

Waite, J. H., Perryman, R. S., Perry, M. E., Miller, K. E., Bell, J. M., Cravens, T. E., et al. (2018). INMS observations of chemical interactions between Saturn's atmosphere and rings. *Science*. https://doi.org/10.1126/science.aat2382

Yelle, R. V., Serigano, J., Koskinen, T. T., Horst, S. M., Perry, M. E., Cravens, T. E., et al. (2018). Thermal structure and composition of Saturn's upper atmosphere from Cassini/INMS measurements. *Geophysical Research Letters*, 45. https://doi.org/10.1029/2018GL078454